Macromolecules

Article

Cite This: Macromolecules 2018, 51, 2395−2400

Photonic Resins: Designing Optical Appearance via Block Copolymer Self-Assembly

Dong-Po Song,[†] Gianni Jacucci,[†] Feyza Dundar,[‡] Aditi Naik,[‡] Hua-Feng Fei,[‡] Silvia Vignolini,*[,†] and James J. Watkins*[,‡]

[†]Department of Chemistry, University of Cambridge, Lensfield Road, Cambridge CB2 1EW, United Kingdom

[‡]Department of Polymer Science and Engineering, University of Massachusetts Amherst, 120 Governors Drive, Amherst, Massachusetts 01003, United States

Supporting Information

ABSTRACT: Despite a huge variety of methodologies having been proposed to produce photonic structures by self-assembly, the lack of an effective fabrication approach has hindered their practical uses. These approaches are typically limited by the poor control in both optical and mechanical properties. Here we report photonic thermosetting polymeric resins obtained through brush block copolymer (BBCP) self-assembly. We demonstrate that the control of the interplay between order and disorder in the obtained photonic structure offers a powerful tool box for designing the optical appearance of the polymer resins in terms of reflected wavelength and scattering properties. The obtained materials exhibit excellent mechanical properties with hardness up to 172 MPa and Young's modulus over 2.9 GPa, indicating great potential for practical uses as photonic coatings on a variety of surfaces.

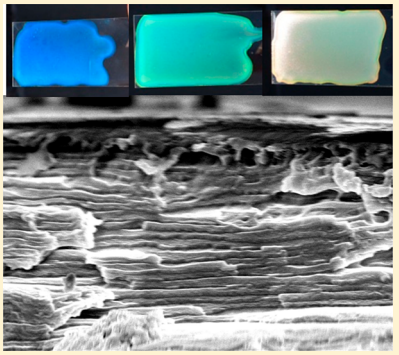

Block copolymer self-assembly is a promising route to the fabrication of photonic materials in a scalable and cost-effective manner.[1−4] Periodic lamellar, cylindrical, bicontinuous, and spherical morphologies are readily accessible for building photonic structures.[5−20] However, their use in real applications remains challenging due to the difficulties in achieving coloration in the visible range on a large scale, the slow kinetics of the self-assembly process, and their poor tolerance toward loadings of additives. Many of these problems can be circumvented by using brush block copolymers (BBCPs),[21−30] as they exhibit substantially reduced polymer chain entanglements relative to their linear analogues, allowing rapid self-assembly kinetics (<5 min), large lattice parameters (>100 nm) on the macroscopic scale, and high loading of functional additives (>70 wt %).[31−36] These advantages come, however, at the cost of mechanical performances; the lack of polymer chain entanglements leads to reduced mechanical strength of such BBCPs relative to their linear analogues.

In the past two decades, BCPs have been used to fabricate nanostructured thermosetting polymer resins and enhance their mechanical properties.[37−40] However, no structural color can be observed from these composites, and coloration of polymer resins typically requires toxic dyes, which can raise environmental concerns. In this work, we create colorful polymer resins via directed self-assembly of phenol formaldehyde resin precursors (PF resols) using amphiphilic BBCPs. We demonstrate that the color appearance (in terms of both reflection and scattering properties) can be tuned by changing the molecular weight of the BBCP or the weight ratio of resol and BBCP. The resulting photonic resins after thermal curing exhibit good mechanical properties such as hardness up to 172 MPa and Young's modulus over 2.9 GPa and thus are suitable for applications in large-area coatings.

RESULTS AND DISCUSSION

Preparation of Photonic Resins with Controlled Optical Appearance. As shown in Figure 1, (polynorbornene-*graft*-poly(*tert*-butyl acrylate))-*block*-(polynorbornene-*graft*-poly(ethylene oxide)) (PtBA-*b*-PEO) BBCPs were selected as the templates for the directed self-assembly of PF resol. The synthesis and characterizations of the BBCPs have been reported in our previous publications,[33] and the molecular weights of the PtBA and PEO brushes are 8.2 and 5.0 kg/mol, respectively. Two representative BBCPs with low and high molecular weights, L-BBCP (2150 kg/mol) and H-BBCP (2760 kg/mol), were selected for the preparation of photonic PF resins with controlled optical appearances. Detailed molecular weight information for the BBCPs is provided in Table S1 (Supporting Information). The PF resol was synthesized according to a reported procedure, yielding a low molecular weight sample (M_n < 500) that is soluble in tetrahydrofuran (THF).[41] For the preparation of the photonic resins, a BBCP and the PF resol are simply mixed in THF followed by self-assembly and thermal curing. The strong hydrogen-bonding interactions between PF resol and the PEO domain enable the selective incorporation of resol within the

Received: October 28, 2017
Revised: March 9, 2018
Published: March 15, 2018

DOI: 10.1021/acs.macromol.7b02288
Macromolecules 2018, 51, 2395−2400

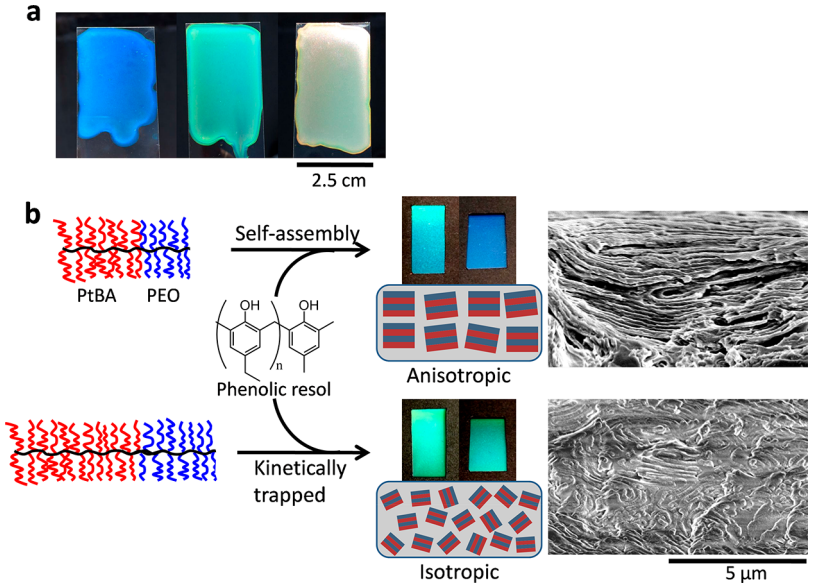

Figure 1. (a) Colorful cross-linked PF resins via the self-assembly of composites containing PtBA-*b*-PEO H-BBCP and PF resol of different concentrations from left to right: 20, 30, and 40 wt %. Thermal curing was performed at 100 °C for 24 h after self-assembly. The photographs were taken on a dark background under sunlight. (b) Control over the self-assembled nanostructures and optical appearances (angle dependent or independent) by using BBCPs with low or high molecular weights. The concentrations of PF resol within the L- and H-BBCP composite samples are 40 and 30 wt %, respectively. Cross-sectional SEM micrographs show the structural difference between well-aligned (anisotropic) and randomly oriented (isotropic) structures.

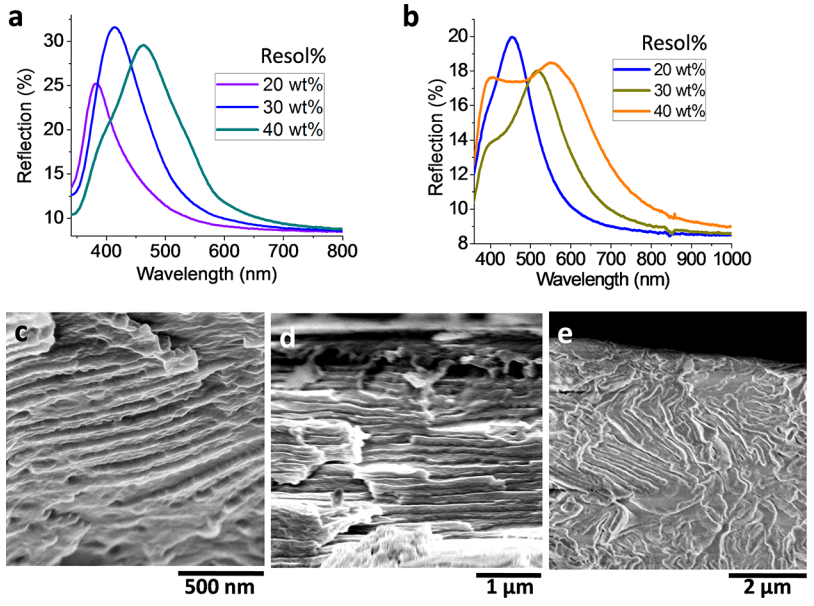

Figure 2. (a, b) Reflection spectra of PF resins containing (a) L-BBCP (M_n = 2150 kg/mol, PDI = 1.08, f_{PEO} = 32.7 vol %) and (b) H-BBCP (M_n = 2760 kg/mol, PDI = 1.05, f_{PEO} = 29.0 vol %), showing a red-shift of the primary peak when increasing the resol concentration. (c–e) Cross-sectional SEM micrographs of composite samples containing different amounts of resol relative to the whole composites: (c) L-BBCP/20 wt % PF, (d) L-BBCP/30 wt % PF, and (e) H-BBCP/40 wt % PF.

hydrophilic domain, forming self-assembled lamellar nanostructures with lattice constant comparable with visible light wavelength. The orientation of such layered structures strongly depends on interactions with interfaces while the grain size depends on dynamics and the competition between nucleation and growth, which are dictated in part by the details of the BBCP and the additives including (i) the molecular weight of the BBCP and (ii) the concentration of PF resol within the composites as well as by the processing conditions.[42] During self-assembly, different nucleation sites for the growth of lamella structures are formed during solvent evaporation, and their orientation is typically random in bulk. However, at the interfaces, anchoring favors the orientation of the lamellar structure parallel to the solution–air or solution–glass interface.[42] As the solvent is gradually removed such that the aggregates become more and more kinetically trapped, the complex drying dynamics (anchoring, gradient of concentration, surface tension, wetting, evaporation front, capillary forces, etc.) plays an important role in the final distribution of the grain size and layer tilting.[43,44] For instance, we can

DOI: 10.1021/acs.macromol.7b02288
Macromolecules 2018, 51, 2395–2400

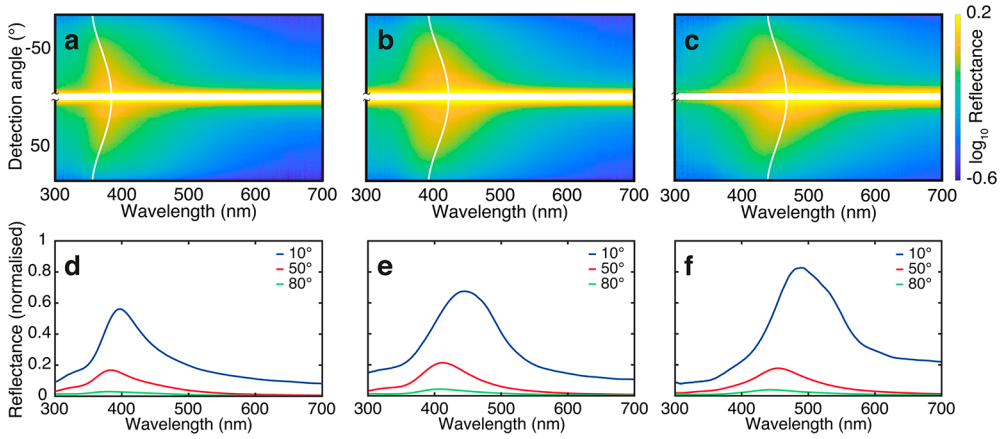

Figure 3. Angular distribution of scattered light from L-BBCP samples, taken with fixed normal incidence. The samples contains different amounts of resol used for sample preparation: (a, d) 20, (b, e) 30, and (c, f) 40 wt %, respectively. (a–c) False-color plots of scattered light intensities. The white curves represent the best fit of the experimental data using Fergason's equation. The data region between −8° and 8° is left blank due to mechanical limits of the experimental setup. (d–f) Line plots of scattered intensities at three different angles corresponding to the false-color plots (a–c), respectively.

fabricate structures with a higher degree of long-range order (larger grain sizes and more aligned domains) using the L-BBCP relative to that of the H-BBCP, which is expected to exhibit slower dynamics during the self-assembly process (see Figure 1b).

As the optical response of lamellar structures is intrinsically angular dependent, it becomes clear that a different orientation of the lamellae composing the resins will provide a different scattering response. Therefore, by changing the two main parameters affecting the dynamics of grain growth and alignment, it is possible to design their optical appearance in terms of both directionality and color response, from vivid colored film (iridescent to matt) to white (see Figure 1a). Figure 1b illustrates in more detail how the interplay between isotropy and anisotropy in the distribution of the lamellae orientation affects the visual appearance of the photonic resins.

When the orientation of the lamellar domains is uniform within the resin, the optical response is very similar to a perfect multilayer, and the optical response follows Bragg's law:[45]

$$\lambda = 2nd \cos\theta \quad (1)$$

where n is the average refractive index, d is the lattice constant, and θ is the angle of incident light with the respect normal to the lamellar orientation. Therefore, as the angle of incidence increases the color blue-shift, see the upper row in Figure 1b. In the case where the distribution of the orientation of the lamellae is random and grain size is small, the appearance of the photonic resin is less angular dependent (see bottom row in Figure 1b). Intuitively, this can be understood by considering that for every observed direction it is possible to find a grain in which the lamellar structure is perpendicular to the incident light; therefore, the predominant color remains similar for all the angles. However, the molecular weight of the BBCP and the amount of PF also affect the lattice spacing d of the lamellae and the refractive index n (see Table S2 and Figure S1), shifting the reflection peak. We therefore chose the two different BBCPs with differed molecular weights, which are labeled as L-BBCP and H-BBCP.

Optical Properties and Structure Characterization. Figure 2a,b shows the optical behavior of the two BBCPs, as the concentration of PF resol increases from 20 to 30 to 40 wt %. All the reflection spectra reported in Figure 2 are measured over a large area (105 mm^2) of the samples using an integrating sphere at an incident angle of 8°, so that all the reflected light at different angles are collected at the same time, independently of the orientation of the lamellae. For both L-BBCP and H-BBCP, we observe that the increase of PF resol leads to gradual red-shift of the reflection maximum. Such spectral behavior can be explained by the swelling of the PEO domain in the presence of the PF resol and the concurrently increased refractive index due to the increased PF resol; for the latter case see Figure S1. However, the red-shift in the case of the H-BBCP is slightly higher than that of the L-BBCP probably because a larger molecular weight accommodates a larger swelling.

By comparing the spectra for the two BBCPs, we notice that the width of the peak becomes larger as the concentration of PF resol is increased and as the molecular weight of the polymer is increased. These phenomena can be best explained as follows: as the BBCP molecular weight or the resol concentration increased, the composite system is more kinetically arrested due to the reduced polymer chain mobility before the system achieved a thermodynamically preferred orientation parallel to the film surface.[42−44]

Figure 2c,d shows cross-sectional SEM micrographs for the L-BBCP samples in which well-ordered lamellar structures can be clearly identified. As expected, the distribution of the lamellae orientation is not perfectly uniform throughout the depth of the film, and as the PF concentration increases, the orientation of the domains becomes increasingly random. In particular, the lamellae structures oriented parallel to the film surface are observed at interface with the air and substrate, while less aligned layers are present in the center of the film (Figure S2) due to reduced interfacial effects. The effect is even more drastic in the case of the H-BBCP. For the sample containing 40 wt % of PF resol, the orientation of layered domains is completely random that the appearance of the film in diffused illumination environment becomes white (see Figure 1a). SEM images of the randomly oriented lamellae for the white sample are reported in Figure 2e and Figure S3.

To further characterize the scattering properties of the film, we performed an angular resolved optical characterization, the experimental setup and data for H-BBCP samples are reported in Figure S4.[46,47] In particular, the incident light illuminate the sample with a fixed θ_{in} = 0 (normal to the film surface), while

DOI: 10.1021/acs.macromol.7b02288
Macromolecules 2018, 51, 2395−2400

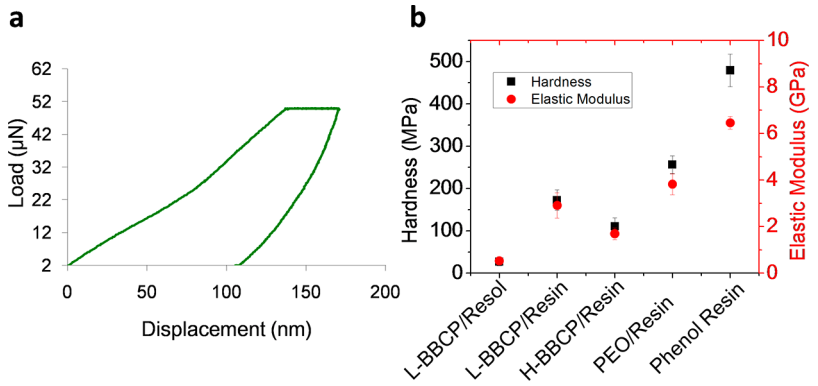

Figure 4. (a) Load/unload−displacement curve of a nanoindentation test on a cured photonic resin film using a three-side pyramidal Berkovich diamond indenter. (b) Hardness and elastic modulus of different BBCP composite samples containing 40 wt % PF resin before and after thermal curring, i.e., L-BBCP/resol and L-BBCP/resin represent samples before and after thermal curing, respectively. The PEO/resin blend contains approximately 70 wt % PF resol, corresponding to about 40 wt % of PF resol within the BBCP composites.

the intensity of the light scattered is acquired at different θ_{out} via detector mounted on a rotating arm. The fact that some light is observed at angle different from $\theta_{out} = 0$ confirmed the presence of tilted domains, i.e., domains whose normal differs from the normal to the sample surface. In fact, each angular point in the color maps in Figure 3a−f results from the specular reflection from a tilted lamellar grain. Moreover, the scattered intensity increases with a decrease of the detection angle, indicating qualitatively that most of the domains have only a small tilting angle relative to the surface normal. In the case where the disorder is not very strong the wavelength of the main reflection peak follows the Fergason's equation:[48,49]

$$\lambda = 2nd\cos\left\{\frac{1}{2}\left[\sin^{-1}\left(\frac{1}{n}\sin\theta_{in}\right) + \sin^{-1}\left(\frac{1}{n}\sin\theta_{out}\right)\right]\right\} \quad (2)$$

where θ_{in} and θ_{out} are the incident and detection angles, respectively.

For the L-BBCP samples, eq 2 fits the experimental data nicely as shown in Figure 3a−c and Figure S5. Therefore, we conclude that the periodicity of the lamellae is constant within the film. The theoretical fit also indicates that the periodicity of the lamellar structure increases with the increased resol loading. In particular, the sample with 40 wt % of PF resol shows a domain spacing of approximately 185 nm, which is 20 nm larger than the one extrapolated for the sample with 20 wt % of the cross-linker. The larger lattice spacing and the increased refractive index (see Figure S1) lead to a red-shift of reflection maximum of almost 120 nm, which consequently results in the different macroscopic coloration of the samples. The loading concentration of PF resol not only influences the periodicity of the lamellar structure but also affects the peak shape as shown in Figure 3e,f. Broader peaks were observed in the reflection spectra for samples with higher PF concentrations. This effect is more evident for H-BBCP samples (Figure S4), suggesting an increased degree of randomly tilted lamellar grains and the distribution of domain spacing—the latter due to the fact that the solvent evaporation after the point of kinetic arrest leads to a quasi-unidirectional compression of the lamellae along the vertical axis.

Mechanical Properties of the Photonic Resins. The mechanical properties of these photonic resin films were characterized by nanoindentation test (see Experimental Section), and 30 indentations were conducted by using three-side pyramidal Berkovich diamond indenter of 100 nm tip radius on each sample. Figure 4a shows a typical load/unload−displacement curve from which both hardness and elastic modulus can be directly obtained or calculated. As shown in Figure 4b, the mechanical strength of the film (L-BBCP) containing 40 wt % of PF resol was greatly enhanced via thermal curing, as indicated by the significantly increased hardness (26.7 vs 172 MPa) and elastic modulus (0.528 vs 2.91 GPa). The modulus achieved is comparable to those of widely used polymer materials, such as polypropylene (PP) and poly(ethylene terephthalate) (PET). For the sample based on H-BBCP containing the same concentration of PF resol, the modulus (1.69 GPa) is evidently lower than that of the L-BBCP sample. This may be best explained by their structural difference. A disordered structure in the H-BBCP sample affords for more mechanical contributions in the Z direction from the soft PtBA domains relative to that from a well-aligned lamellar structures (Figure 3d) observed for the L-BBCP sample film. The mechanical strength of the PEO/resin domain was evaluated by using PEO homopolymer composites containing the corresponding amount of PF resol. As shown in Figure 4b, the modulus of BBCP samples is lower than that of the PEO homopolymer composite sample due to the presence of the soft PtBA domains in the BCP samples. As expected, the cross-linked PF resin film shows the highest elastic modulus based on the nanoindentation test.

CONCLUSIONS

In summary, we have demonstrated an effective strategy for fabricating thermosetting photonic resins via BCP self-assembly. Without pigments, these polymer resin films exhibit vivid colors by forming lamellar structures that are large enough to reflect visible light. The optical appearances, in terms of reflection and scattering, can be tuned via the control of the self-assembly kinetics. The obtained polymer resins after thermal curing show excellent mechanical properties that are comparable to those of widely used polymer materials. Therefore, the photonic resins are promising for use in many applications such as decoration coatings, photonic papers, optical filters, and security labeling. The composite materials are simply prepared in solutions that can be further processed by roll-to-roll or inject printing techniques, offering new opportunities for scalable fabrication of cost-effective photonic materials.

DOI: 10.1021/acs.macromol.7b02288
Macromolecules 2018, 51, 2395−2400

EXPERIMENTAL SECTION

Preparation of BBCP Composite Samples. Appropriate amounts of brush block copolymers were weighed and dissolved in tetrahydrofuran (THF) followed by adding PF resol solutions in the same solvent to form about 4.0% (w/v) stock solutions. The THF solutions were cast through 0.45 μm PTFE filters onto horizontal glass substrates which were covered immediately with glass Petri dishes, and the dried films after evaporation at room temperature for about 4 h were put under vacuum at 100 °C for about 24 h to completely remove a trace amount of residual solvent and to make cross-linked photonic resin. We note that the evaporation of THF solutions was carried out under a nitrogen atmosphere to control humidity below 20%.

Preparation of PEO/Resin Homopolymer Blends. PEO (2 kg/mol) from Sigma was blended with the PF resol in THF at different loading concentrations. The concentration of the resulting solution was around 10 mg/mL. Thin films on silicon substrate for variable angle spectroscopic ellipsometry (VASE) measurements were prepared by spin-coating at 3000 rpm, affording film thicknesses ranging from 73 to 83 nm. The thin films were subsequently thermally cured at 100 °C for 24 h before VASE measurements.

Characterization. *Field Emission Scanning Electron Microscopy (FESEM).* FESEM measurements were carried out on a FEI Magellan 400 FESEM. The composites samples on glass substrates were fractured at room temperature to afford the cross sections for SEM. A thin layer of platinum of approximately 1 nm was coated on the samples before SEM characterizations using a sputtering coater.

Reflection Measurements. These measurements of the samples were performed on a PerkinElmer LAMBDA 1050 UV/vis/NIR spectrometer, equipped with a 150 mm integrating sphere diffuse reflectance accessory. All measurements were referenced to a Spectralon reflectance standard with a 99% reflection. The light beam size was 7 mm in width and 15 mm in length.

Variable Angle Spectroscopic Ellipsometry (VASE). VASE measurements were performed on a J.A. Woollam RC2-DI ellipsometry with variable angles at 55°, 60°, 65°, and 70°. The refractive index was obtained by using a Cauchy model for data fitting.

Angular Distribution of Scattered/Transmitted Light. The angular distribution was determined using a goniometer setup. The samples were illuminated using a xenon lamp Ocean Optics HPX-2000 coupled into an optical fiber (Thorlabs FC-UV100-2-SR). The illumination angle was fixed at normal incidence, and the angular distribution of intensity was acquired moving the detector arm with a resolution of 1°. The detector was moved over an interval of 180° around the normal incidence direction. The detector used for this setup was a 600 μm core fiber (Thorlabs FC-UV600-2-SR) connected to a spectrometer (Avantes HS2048). The spectra were acquired with an integrating time of 0.1 s and averaged over 10 acquisitions. The experimental data were normalized against a standard white diffuser (Labsphere SRS-99-010).

Hysitron Nanoindenter. The nanoindenter was used to measure hardness and reduced modulus (E_r). All the measurements were done as rate control (10 μN/s); 30 indentations were conducted by using three-side pyramidal Berkovich diamond indenter of 100 nm tip radius on each sample. Indentation contact depth was kept less than 10% of the film thickness in order to prevent substrate effect and higher than 40 nm to have meaningful results. Each nanoindentation test was conducted 20 μm separate from each other at a new location to avoid possible interferences. We followed the Oliver and Pharr method to determine hardness and modulus. The elastic modulus or Young's modulus was calculated according to eq 3:[50]

$$\frac{1}{E_r} = \frac{1-\nu^2}{E} + \frac{1-\nu_i^2}{E_i} \tag{3}$$

where E and ν are Young's modulus and Poisson's ratio for the specimen and E_i and ν_i are the same parameters for the diamond indenter. The elastic modulus of the Berkovich indenter tip (1140 GPa) is orders of magnitude larger than the elastic modulus of the sample, and the second term in eq 3 is negligible. Therefore, eq 3 can be simplified as the expression $E = E_r(1 - \nu^2)$, where the Poisson's ratio of polymer materials is approximately 0.3.

ASSOCIATED CONTENT

Supporting Information

The Supporting Information is available free of charge on the ACS Publications website at DOI: 10.1021/acs.macromol.7b02288.

Information table for the polymers, VASE data, SEM images, and angular distribution of scattered light (PDF)

AUTHOR INFORMATION

Corresponding Authors

*(S.V.) E-mail sv319@cam.ac.uk; Tel +44 1223 761490.

*(J.J.W.) E-mail watkins@polysci.umass.edu; Tel +1 (413) 545-2569.

ORCID

Dong-Po Song: 0000-0002-2825-4999

Notes

The authors declare no competing financial interest.

ACKNOWLEDGMENTS

This work was supported by the NSF Center for Hierarchical Manufacturing at the University of Massachusetts (CMMI-1025020), a BBSRC David Phillips Fellowship [BB/K014617/1], and the European Research Council [ERC-2014-STG H2020 639088] at the University of Cambridge.

REFERENCES

(1) Fink, Y.; Urbas, A. M.; Bawendi, M. G.; Joannopoulos, J. D.; Thomas, E. L. Block Copolymers as Photonic Bandgap Materials. *J. Lightwave Technol.* **1999**, *17*, 1963−1969.

(2) Valkama, S.; Kosonen, H.; Ruokolainen, J.; Haatainen, T.; Torkkeli, M.; Serimaa, R.; ten Brinke, G.; Ikkala, O. Self-Assembled Polymeric Solid Films with Temperature-Induced Large and Reversible Photonic-Bandgap Switching. *Nat. Mater.* **2004**, *3*, 872−876.

(3) Kang, Y.; Walish, J. J.; Gorishnyy, T.; Thomas, E. L. Broad-Wavelength-Range Chemically Tunable Block-Copolymer Photonic Gels. *Nat. Mater.* **2007**, *6*, 957−960.

(4) Lee, J.-H.; Koh, C. Y.; Singer, J. P.; Jeon, S.; Maldovan, M.; Stein, O.; Thomas, E. L. Ordered Polymer Structures for The Engineering of Photons and Phonons. *Adv. Mater.* **2014**, *26*, 532−569.

(5) Bates, F. S.; Hillmyer, M. A.; Lodge, T. P.; Bates, C. M.; Delaney, K. T.; Fredrickson, G. H. Multiblock Polymers: Panacea or Pandora's Box? *Science* **2012**, *336*, 434−440.

(6) Park, C.; Yoon, J.; Thomas, E. L. Enabling Nanotechnology with Self-Assembled Block Copolymer Patterns. *Polymer* **2003**, *44*, 6725−6760.

(7) Urbas, A. M.; Sharp, R.; Fink, Y.; Thomas, E. L.; Xenidou, M.; Fetters, L. J. Tunable Block Copolymer/Homopolymer Photonic Crystals. *Adv. Mater.* **2000**, *12*, 812−814.

(8) Deng, T.; Chen, C.; Honeker, C.; Thomas, E. L. Two-Dimensional Block Copolymer Photonic Crystals. *Polymer* **2003**, *44*, 6549−6553.

(9) Urbas, A. M.; Maldovan, M.; DeRege, P.; Thomas, E. L. Bicontinuous Cubic Block Copolymer Photonic Crystals. *Adv. Mater.* **2002**, *14*, 1850−1853.

(10) Edrington, A. C.; Urbas, A. M.; DeRege, P.; Chen, C. X.; Swager, T. M.; Hadjichristidis, N.; Xenidou, M.; Fetters, L. J.; Joannopoulos, J. D.; Fink, Y.; Thomas, E. L. Polymer-Based Photonic Crystals. *Adv. Mater.* **2001**, *13*, 421−425.

(11) Kim, E.; Kang, C.; Baek, H.; Hwang, K.; Kwak, D.; Lee, E.; Kang, Y.; Thomas, E. L. Control of Optical Hysteresis in Block

DOI: 10.1021/acs.macromol.7b02288
Macromolecules 2018, 51, 2395−2400

Copolymer Photonic Gels: A Step Towards Wet Photonic Memory Films. *Adv. Funct. Mater.* **2010**, *20*, 1728−1732.
(12) Lim, H. S.; Lee, J.-H.; Walish, J. J.; Thomas, E. L. Dynamic Swelling of Tunable Full-Color Block Copolymer Photonic Gels via Counter ion Exchange. *ACS Nano* **2012**, *6*, 8933−8939.
(13) Noro, A.; Tomita, Y.; Shinohara, Y.; Sageshima, Y.; Walish, J. J.; Matsushita, Y.; Thomas, E. L. Photonic Block Copolymer Films Swollen with An Ionic Liquid. *Macromolecules* **2014**, *47*, 4103−4109.
(14) Kang, C.; Kim, E.; Baek, H.; Hwang, K.; Kwak, D.; Kang, Y.; Thomas, E. L. Full Color Stop Bands in Hybrid Organic/Inorganic Block Copolymer Photonic Gels by Swelling−Freezing. *J. Am. Chem. Soc.* **2009**, *131*, 7538−7539.
(15) Ge, J.; Yin, Y. Responsive Photonic Crystals. *Angew. Chem., Int. Ed.* **2011**, *50*, 1492−1522.
(16) Galisteo-López, J. F.; Ibisate, M.; Sapienza, R.; Froufe-Pérez, L. S.; Blanco, Á.; López, C. Self-Assembled Photonic Structures. *Adv. Mater.* **2011**, *23*, 30−39.
(17) Wang, J.; Zhang, Y.; Wang, S.; Song, Y.; Jiang, L. Bioinspired Colloidal Photonic Crystals with Controllable Wettability. *Acc. Chem. Res.* **2011**, *44*, 405−415.
(18) Aguirre, C. I.; Reguera, E.; Stein, A. Tunable Colors in Opals and Inverse Opal Photonic Crystals. *Adv. Funct. Mater.* **2010**, *20*, 2565−2578.
(19) Yamanaka, T.; Hara, S.; Hirohata, T. A narrow band-rejection filter based on block copolymers. *Opt. Express* **2011**, *19*, 24583−24588.
(20) Kang, H. S.; Lee, J.; Cho, S. M.; Park, T. H.; Kim, M. J.; Park, C.; Lee, S. W.; Kim, K. L.; Ryu, D. Y.; Huh, J.; Thomas, E. L.; Park, C. Printable and Rewritable Full Block Copolymer Structural Color. *Adv. Mater.* **2017**, *29*, 1700084−1700088.
(21) Mapas, J. K. D.; Thomay, T.; Cartwright, A. N.; Ilavsky, J.; Rzayev, J. Ultrahigh Molecular Weight Linear Block Copolymers: Rapid Access by Reversible-Deactivation Radical Polymerization and Self-Assembly into Large Domain Nanostructures. *Macromolecules* **2016**, *49*, 3733−3738.
(22) Rzayev, J. Molecular Bottlebrushes: New Opportunities in Nanomaterials Fabrication. *ACS Macro Lett.* **2012**, *1*, 1146−1149.
(23) Liberman-Martin, A. L.; Chu, C. K.; Grubbs, R. H. Application of Bottlebrush Block Copolymers As Photonic Crystals. *Macromol. Rapid Commun.* **2017**, *38*, 1700058.
(24) Rzayev, J. Synthesis of Polystyrene-Polylactide Bottlebrush Block Copolymers and Their Melt Self-Assembly into Large Domain Nanostructures. *Macromolecules* **2009**, *42*, 2135−2141.
(25) Xia, Y.; Olsen, B. D.; Kornfield, J. A.; Grubbs, R. H. Efficient Synthesis of Narrowly Dispersed Brush Copolymers and Study of Their Assemblies: The Importance of Side Chain Arrangement. *J. Am. Chem. Soc.* **2009**, *131*, 18525−18532.
(26) Sveinbjörnsson, B. R.; Weitekamp, R. A.; Miyake, G. M.; Xia, Y.; Atwater, H. A.; Grubbs, R. H. Rapid Self-Assembly of Brush Block Copolymers to Photonic Crystals. *Proc. Natl. Acad. Sci. U. S. A.* **2012**, *109*, 14332−14336.
(27) Miyake, G. M.; Piunova, V. A.; Weitekamp, R. A.; Grubbs, R. H. Precisely Tunable Photonic Crystals from Rapidly Self-Assembling Brush Block Copolymer Blends. *Angew. Chem., Int. Ed.* **2012**, *51*, 11246−11248.
(28) Piunova, V. A.; Miyake, G. M.; Daeffler, C. S.; Weitekamp, R. A.; Grubbs, R. H. Highly Ordered Dielectric Mirrors via The Self-Assembly of Dendronized Block Copolymers. *J. Am. Chem. Soc.* **2013**, *135*, 15609−15616.
(29) Macfarlane, R. J.; Kim, B.; Lee, B.; Weitekamp, R. A.; Bates, C. M.; Lee, S. F.; Chang, A. B.; Delaney, K. T.; Fredrickson, G. H.; Atwater, H. A.; Grubbs, R. H. Improving Brush Polymer Infrared One-Dimensional Photonic Crystals via Linear Polymer Additives. *J. Am. Chem. Soc.* **2014**, *136*, 17374−17377.
(30) Boyle, B. M.; French, T. A.; Pearson, R. M.; McCarthy, B. G.; Miyake, G. M. Structural Color for Additive Manufacturing: 3D-Printed Photonic Crystals from Block Copolymers. *ACS Nano* **2017**, *11*, 3052−3058.
(31) Yavitt, B. M.; Gai, Y.; Song, D.-P.; Winter, H. H.; Watkins, J. J. Molecular Mobility in Phase Segregated Bottlebrush Block Copolymer Melts. *Macromolecules* **2017**, *50*, 396−405.
(32) Song, D. P.; Shahin, S.; Xie, W.; Mehravar, S.; Liu, X.; Li, C.; Norwood, R. A.; Lee, J.-H.; Watkins, J. J. Directed Assembly of Quantum Dots Using Brush Block Copolymers for Well-Ordered Nonlinear Optical Nanocomposites. *Macromolecules* **2016**, *49*, 5068−5075.
(33) Song, D. P.; Li, C.; Li, W.; Watkins, J. J. Block Copolymer Nanocomposites with High Refractive Index Contrast for One-Step Photonics. *ACS Nano* **2016**, *10*, 1216−1223.
(34) Song, D. P.; Li, C.; Colella, N. S.; Lu, X.; Lee, J. H.; Watkins, J. J. Thermally Tunable Metallodielectric Photonic Crystals from The Self-Assembly of Brush Block Copolymers and Gold Nanoparticles. *Adv. Opt. Mater.* **2015**, *3*, 1169−1175.
(35) Song, D. P.; Lin, Y.; Gai, Y.; Colella, N. S.; Li, C.; Liu, X. H.; Gido, S.; Watkins, J. J. Controlled Supramolecular Self-Assembly of Large Nanoparticles in Amphiphilic Brush Block Copolymers. *J. Am. Chem. Soc.* **2015**, *137*, 3771−3774.
(36) Song, D. P.; Li, C.; Colella, N. S.; Xie, W.; Li, S.; Lu, X.; Gido, S.; Lee, J. H.; Watkins, J. J. Large-Volume Self-Organization of Polymer/Nanoparticle Hybrids with Millimeter-Scale Grain Sizes Using Brush Block Copolymers. *J. Am. Chem. Soc.* **2015**, *137*, 12510−12513.
(37) Lipic, P. M.; Bates, F. S.; Hillmyer, M. A. Nanostructured Thermosets from Self-Assembled Amphiphilic Block Copolymer/Epoxy Resin Mixtures. *J. Am. Chem. Soc.* **1998**, *120*, 8963−8970.
(38) Mijovic, J.; Shen, M.; Wing Sy, J.; Mondragon, I. Dynamics and Morphology in Nanostructured Thermoset Network/Block Copolymer Blends during Network Formation. *Macromolecules* **2000**, *33*, 5235−5244.
(39) Liu, J.; Sue, H. J.; Thompson, Z. J.; Bates, F. S.; et al. Nanocavitation in Self-Assembled Amphiphilic Block Copolymer-Modified Epoxy. *Macromolecules* **2008**, *41*, 7616−7624.
(40) Amendt, M. A.; Chen, L.; Hillmyer, M. A. Formation of Nanostructured Poly(dicyclopentadiene) Thermosets Using Reactive Block Polymers. *Macromolecules* **2010**, *43*, 3924−3934.
(41) Meng, Y.; Gu, D.; Zhang, F.; Shi, Y.; Cheng, L.; Feng, D.; Wu, Z.; Chen, Z.; Wan, Y.; Stein, A.; Zhao, D. A Family of Highly Ordered Mesoporous Polymer Resin and Carbon Structures from Organic-Organic Self-Assembly. *Chem. Mater.* **2006**, *18*, 4447−4464.
(42) Darling, S. B. Directing The Self-Assembly of Block Copolymers. *Prog. Polym. Sci.* **2007**, *32*, 1152−1204.
(43) Mai, Y.; Eisenberg, A. Self-Assembly of Block Copolymers. *Chem. Soc. Rev.* **2012**, *41*, 5969−5985.
(44) Parker, R.; Frka-Petesic, B.; Guidetti, G.; Kamita, G.; Consani, G.; Abell, C.; Vignolini, S. Hierarchical Self-Assembly of Cellulose Nanocrystals in A Confined Geometry. *ACS Nano* **2016**, *10*, 8443−8449.
(45) Bragg, W. The Diffraction of Short Electromagnetic Waves by Crystals. *Proc. Cambridge Philos. Soc.* **1913**, *17*, 43−57.
(46) Vignolini, S.; Moyroud, E.; Glover, B. J.; Steiner, U. Analysing Photonic Structures in Plants. *J. R. Soc., Interface* **2013**, *10*, 20130394.
(47) Kamita, G.; Frka-Petesic, B.; Allard, A.; Dargaud, M.; King, K.; Dumanli, A. G.; Vignolini, S. Biocompatible and Sustainable Optical Strain Sensors for Large-Area Applications. *Adv. Opt. Mater.* **2016**, *4*, 1950−1954.
(48) Fergason, J. L. Cholesteric Structure-1 Optical Properties. *Mol. Cryst.* **1966**, *1*, 293−307.
(49) Werbowyj, R. S.; Gray, D. G. Optical Properties of Hydroxypropyl Cellulose Liquid Crystals. I. Cholesteric Pitch and Polymer Concentration. *Macromolecules* **1984**, *17*, 1512−1520.
(50) Oliver, W. C.; Pharr, G. M. An Improved Technique for Determining Hardness and Elastic Modulus Using Load and Displacement Sensing Indentation Experiments. *J. Mater. Res.* **1992**, *7*, 1564−1583.

DOI: 10.1021/acs.macromol.7b02288
Macromolecules 2018, 51, 2395−2400